Nano Research
2020, 13(3): 729–735
ISSN 1998-0124 CN 11-5974/O4
https://doi.org/10.1007/s12274-020-2683-2

Research Article

Intrinsic defects in biomass-derived carbons facilitate electroreduction of CO_2

Mengjie Chen[1], Shuai Wang[1], Haiyan Zhang[1], Ping Zhang[1], Ziqi Tian[2] (✉), Min Lu[1] (✉), Xiaoji Xie[1] (✉), Ling Huang[1], and Wei Huang[1,3]

[1] *Key Laboratory of Flexible Electronics (KLOFE), Institute of Advanced Materials (IAM), Nanjing Tech University, Nanjing 211816, China*
[2] *Ningbo Institute of Materials Technology and Engineering, Chinese Academy of Sciences, Ningbo 315201, China*
[3] *Shaanxi Institute of Flexible Electronics, Northwestern Polytechnical University, Xi'an 710072, China*

Received: 12 November 2019 / **Revised:** 20 January 2020 / **Accepted:** 23 January 2020

ABSTRACT

Developing efficient carbon-based metal-free electrocatalysts can bridge the gap between laboratory studies and practical applications of CO_2 reduction. However, along with the ambiguous understanding of the active sites in carbon-based electrocatalysts, carbon-based electrocatalysts with high selectivity and satisfactory stability for electroreduction of CO_2 remain rare. Here, using the nitrogen rich silk cocoon as a precursor, carbon-based electrocatalysts with intrinsic defects can be prepared for efficient and long-term electroreduction of CO_2 by a simple two-step carbonization. The obtained electrocatalyst can catalyze CO_2 reduction to CO with a Faradaic efficiency of ~ 89% and maintain good selectivity for about 10 days. Particularly, our experimental studies suggest that in-plane defects are the main active sites on which the rate-determining step for CO_2 reduction should be the direct electron transfer to CO_2 but not the proton-coupled electron transfer. Further theoretical calculations consistently demonstrate that the intrinsic defects in carbon matrix, particularly the pentagon-containing defects, act as main active sites to accelerate the direct electron transfer for CO_2 reduction. In addition, our synthetic approach can convert egg white into efficient catalysts for CO_2 electroreduction. These findings, providing new insights into the biomass-derived catalysts, should pave the way for fabricating efficient and stable carbon-based electrocatalysts with catalytically active defects by using naturally abundant precursors.

KEYWORDS

carbon dioxide, reduction, carbon-based catalyst, defect, biomass

1 Introduction

Electroreduction of carbon dioxide (CO_2), which can convert CO_2 molecules into high-value products, is an appealing means to alleviate energy crisis and environmental issues caused by evergrowing CO_2 [1–3]. Because of the sluggish CO_2 reduction reaction (CO_2RR), electrocatalysts are needed during the electroreduction of CO_2 [4]. Currently, the commonly used electrocatalysts for CO_2RR are based on metals, including Au, Pd, Ag, and Cu [4, 5]. However, the metal-based electrocatalysts typically suffer from several weaknesses, such as high cost, low abundance, and unsatisfactory stability [4]. Carbon-based electrocatalysts [6], a type of metal-free catalysts, recently emerge as alternatives for electroreduction of CO_2. Compared with those metal-based electrocatalysts [5], carbon-based electrocatalysts have intrinsic advantages, including low cost, natural abundance, tunable morphology, and excellent thermal/chemical stability [7, 8].

Basically, carbon materials, such as pristine graphene, do not exhibit catalytic activity for electrocatalytic reactions, including CO_2RR [9]. The most commonly used strategy for preparing carbon-based electrocatalysts is the heteroatom doping, particularly N doping, in the carbon matrix [7]. In fact, the majority of present carbon-based electrocatalysts for CO_2RR are the heteroatom-doped carbon electrocatalysts. These catalysts now can convert CO_2 into CO with a high Faradaic efficiency, while their durability is scarcely studied [10–20]. Very recently, the intrinsic carbon defects in carbon matrix, such as intrinsic pentagons, have been proposed as better active sites for electrocatalytic reactions when compared with those in N doped carbon electrocatalysts [21–24]. However, introducing intrinsic defects into carbons, especially in a large-scale and controllable manner, is still challenging [8]. Typically, doping and subsequent removal of N atoms are needed to create intrinsic defects in the carbon matrix [25]. It should also be mentioned that most of the current studies about carbon-based electrocatalysts with intrinsic defects focus on the oxygen reduction and hydrogen evolution reactions, but not CO_2RR [8]. Furthermore, in the limited studies using defect-rich carbon electrocatalysts for CO_2RR catalysis, the long-term stability of these electrocatalysts has not been explored [3].

Biomass is a type of precursor with great abundance for synthesizing carbon-based electrocatalysts, and biomass-derived carbons can be potential electrocatalysts for diverse electrocatalytic reactions [3]. Despite the potential, only a few studies use biomass to fabricate electrocatalysts for CO_2RR, and the underlying catalytic mechanisms are still unclear. Recently, two studies showed that biomass carbons containing N, derived from wood and wheat, can assist the conversion of

Address correspondence to Ziqi Tian, tianziqi@nimte.ac.cn; Min Lu, iammlv@njtech.edu.cn; Xiaoji Xie, iamxjxie@njtech.edu.cn

CO_2 into CO, and they attributed the catalytic performance of biomass carbons to the N-doping effect [26, 27]. Taking the typical method for creating intrinsic carbon defects into account, we reason that efficient and stable carbon electrocatalysts with intrinsic defects can be obtained for CO_2RR if biomass with rich N contents is used as the precursor.

In this study, using the silk cocoon as a representative N rich biomaterial, we show that carbon electrocatalysts with intrinsic defects for electroreduction of CO_2 can be derived by a two-step carbonization. The electrocatalyst synthesized under our optimized conditions can convert CO_2 into CO with the CO Faradaic efficiency (FE_{CO}) of ~ 89% at a CO partial geometric current density of ~ 0.8 mA·cm^{-2}. Remarkably, the catalyst exhibits a good stability which can maintain a high FE_{CO} (> 85%) for ~ 10 days. Our experimental results together with density functional theory (DFT) calculations indicate that the intrinsic pentagon-containing defects in the derived catalysts should be the main active sites which significantly accelerate the direct electron transfer to CO_2 and thus the kinetics of CO_2RR. Furthermore, we show that our carbonization approach can be used to convert other biomass, such as egg white, into excellent carbon-based electrocatalysts for CO_2RR. These results imply the feasibility of using N-rich biomass for fabricating carbon electrocatalysts with high efficiency and remarkable stability for CO_2RR.

2 Experimental

2.1 Materials

Potassium bicarbonate ($KHCO_3$, 99.5%) was purchased from General-Reagent Co., Ltd. Zinc chloride ($ZnCl_2$, 98%) was purchased from Shanghai Xinbao Fine Chemical Co., Ltd. Hydrochloric acid (HCl, 36%–38%) was purchased from Shanghai Lingfeng Chemical Reagent Co., Ltd. Nafion (5%) was purchased from Shanghai Hessen Electric Co., Ltd. Carbon plate was purchased from Beijing Jing Long Te Tan Technology Co. Ltd. Silk cocoon was purchased from Taobao (shop id: 66007777). Anhydrous ethanol was purchased from Sinopharm Chemical Reagent Co., Ltd. Deionized water was produced from a Millipore Direct-Q8. Unless otherwise noted, all chemicals were used as received without further purification.

2.2 Synthesis of biomass-derived electrocatalysts

Generally, the biomass-derived electrocatalysts were synthesized by a two-step carbonization method. In this method, the first step was pre-carbonization that was performed at a selected temperature (T_1). Secondly, the pre-carbonized materials were further activated in the presence of $ZnCl_2$ at a relatively high temperature (T_2). The obtained electrocatalysts were named as A-T_1-T_2, where A, T_1, and T_2 represent activation with $ZnCl_2$, pre-carbonization temperature, and activation temperature, respectively. It should be mentioned that the control sample activated in the absence of $ZnCl_2$, named as NA-T_1-T_2, was also prepared for comparison.

Taking the synthesis of the A-350-1000 electrocatalyst as an example, in a typical synthesis, silk cocoons (4 pieces) were first pre-carbonized at 350 °C for 1 h under steady N_2 flow (~ 10 mL·min^{-1}) in a tube furnace with a ramping rate of 5 °C·min^{-1}. The pre-carbonized silk cocoons were then mixed with $ZnCl_2$ powder in a weight ratio of 1/2 (pre-carbonized silk cocoons:$ZnCl_2$ = 1:2), and the resulting mixture was ground to ensure sufficient mixing. Subsequently, the mixture was activated by further pyrolysis at 1,000 °C for 1 h under steady N_2 flow (~ 10 mL·min^{-1}) in a tube furnace with a ramping rate of 5 °C·min^{-1}. After the mixture was cooled down to room temperature, the obtained carbon powder was immersed in a HCl solution (1.2 mol·L^{-1}) under stirring for 24 h at room temperature in order to remove the Zn-containing residues. Next, the carbon powder was collected, thoroughly washed with deionized water and ethanol, and dried in vacuum at 60 °C for 12 h. Finally, the carbon powder, as the electrocatalyst, was collected and stored for further characterization (more details in the Electronic Supplementary Material (ESM)).

2.3 Electroreduction of CO_2 and electrochemical characterizations

Typically, CO_2 reduction reaction and corresponding electrochemical characterization were carried out in a single-chamber gastight reactor (100 mL) using the three-electrode mode. Specifically, the Ag/AgCl/KCl (KCl: 3 mol·L^{-1}) electrode, a platinum foil, and an electrocatalyst coated carbon plate were used as the reference electrode (0.21 V vs. the standard hydrogen electrode (SHE)), the counter electrode, and the working electrode, respectively. For preparing the working electrode, a mixture containing 5 mg electrocatalyst, 150 μL ethanol, and 20 μL Nafion solution was first ultrasonicated for 30 min to form a uniform dispersion. The mixture was then spin coated onto a carbon plate (1 cm × 2 cm) to achieve a loading of 0.5 mg·cm^{-2}. It should be mentioned that the total weight of the electrocatalyst was 1 mg on two sides of the carbon plate, and the coating was limited in an area of 1 cm × 1 cm on each side. Particularly, an extra area of the carbon plate (1 cm × 1 cm) was designed to guarantee the conductive connection to the electrode holder.

Prior to the electroreduction of CO_2 and corresponding electrochemical characterization, an aqueous solution of $KHCO_3$ (60 mL, 0.1 mol·L^{-1}) was added into the reactor as the electrolyte, leaving a headspace of 40 mL. The electrolyte was then purged with CO_2 or Ar for 30 min to remove air in the headspace. Subsequently, cyclic voltammetry (CV) was carried out on an electrochemical workstation (CHI 660, CH Instruments or IM6, Zahner) for 30 cycles from −0.6 to −2.0 V (vs. the Ag/AgCl/KCl electrode) at a scan rate of 50 mV·s^{-1} to activate and stabilize the catalyst–electrolyte interface. Notably, this potential range can be described as −0.39 to −1.79 V when compared with the SHE. All the potentials reported in this study were referred to the SHE unless otherwise noted.

Linear sweep voltammetry (LSV) was carried out in the range of −0.39 to −1.79 V at a scan rate of 2 mV·s^{-1}. Using the same experimental setup, the electrochemical impedance spectroscopy (EIS) analysis was recorded at different potentials on an electrochemical workstation (IM6, Zahner) in the frequency range of 5 MHz to 10 mHz (amplitude: 5 mV).

To determine the products, gaseous and liquid products, collected from the gastight reactor after electroreduction of CO_2 at constant potentials, were analyzed by gas chromatography (GC-2014 gas chromatograph, Shimazdu) and liquid chromatography (Primaide liquid chromatograph, Hitachi), respectively. Unless otherwise noted, the electrolysis time was 1,800 s for screening different electrocatalysts (Figs. 1(c) and 1(d), and Fig. S9 in the ESM), and 3,600 s for all the other experiments.

To study the long-term stability of the electrocatalyst for CO_2 reduction, a constant potential of −1.09 V was applied on the working electrode. Both the gaseous and liquid products were quantified intermittently during the study (231 h) in order to evaluate the catalytic performance of the electrocatalyst. During the long-term study, the electroreduction of CO_2 was continuously carried out in a reactor with a gas vent under steady CO_2 purging. When the quantitative analysis of the

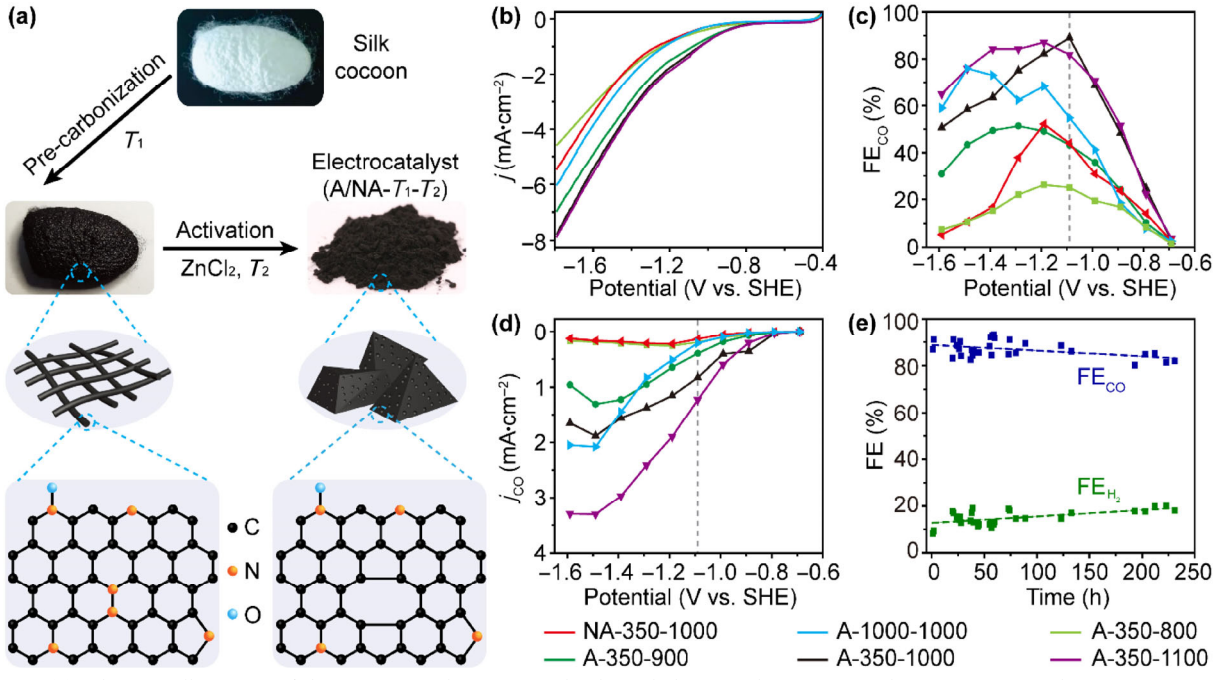

Figure 1 (a) Schematic illustration of the two-step carbonization. The derived electrocatalysts are named as A/NA-T_1-T_2, where A, NA, T_1, and T_2 represent activation with $ZnCl_2$, activation without $ZnCl_2$, pre-carbonization temperature, and activation temperature, respectively. (b) Linear sweep voltammograms of the electrocatalysts in the CO_2 environment. The minus (−) in j values only indicates that the reaction is a reduction reaction. (c) and (d) FE of CO production (FE_{CO}) and j_{CO} as a function of reduction potential by using the electrocatalysts, respectively. (e) Time-dependent FE of CO production, and FE of H_2 production at −1.09 V by using the A-350-1000 electrocatalyst. The dashed lines in (e) are linear fitting of the data to guide the eye. j, j_{CO}, FE, and SHE denote current density, the CO partial current density, Faradaic efficiency, and the standard hydrogen electrode, respectively. The electrochemical measurements were performed in $KHCO_3$ (0.1 mol·L^{-1}, aqueous solution) using the carbon plate loaded with electrocatalysts (0.5 mg·cm^{-2}) unless otherwise noted.

products was required, the reaction was temporarily ceased. Subsequently, the reactor was refilled with fresh electrolyte, purged with CO_2 for 30 min, and sealed for further electroreduction of CO_2. After the reaction was continued for 1 h, both the gaseous and liquid products were collected from the sealed reactor and analyzed. To continue the long-term study, after the collection of products, the gas vent in the reactor was opened immediately and CO_2 was steadily purged into the reactor. Notably, the time used for electrolyte refilling and subsequent CO_2 purging was not added into the time for electroreduction of CO_2. For example, to evaluate the catalytic performance of the electrocatalyst after 20 h, fresh $KHCO_3$ electrolyte (60 mL, 0.1 mol·L^{-1}) was refilled into the reactor after the reaction was kept for 19 h. The reactor was then purged by CO_2 for 30 min and sealed. After 1-h electroreduction of CO_2, the gas and liquid products were collected and analyzed. Notably, the change of electrolyte is to minimize the effects brought by the evaporation of electrolyte during the long-term electrolysis.

2.4 Computational methods

To consider solvation effects and systems with charge, theoretical calculations were carried out by using the Gaussian 09 program package on the basis of fragment models. The computational details are in the ESM.

3 Results and discussion

3.1 Preparation and general characterization of carbon electrocatalysts

The carbon electrocatalysts were prepared by a two-step carbonization approach as shown in Fig. 1(a). In this approach, the first step, pre-carbonization, is performed at 350 °C (T_1 in Fig. 1(a)). Notably, silk cocoon is composed of natural protein fibers with a high N content (~ 15%) [28], and the pre-carbonization at relatively low temperature can transform the β-sheet structure of the protein in the silk cocoon into a conjugated sp^2-hybridized hexagonal carbon structure with N doping [29]. It should also be mentioned that the pre-carbonization temperature was selected according to the thermogravimetric analysis (Fig. S1 in the ESM) and previous studies [29]. Subsequently, an activation process by adding $ZnCl_2$ is carried out at relatively high temperature (T_2 in Fig. 1(a)). We believe that the activation step can create pores in carbons, yielding carbon catalysts with enlarged surface areas and intrinsic defects [30, 31]. Meanwhile, at high temperature, N atoms can be removed to generate intrinsic defects in the carbon matrix [29]. Using this method, a group of carbon electrocatalysts (A-350-T_2) were obtained at different activation temperature (T_2 = 800, 900, 1,000, and 1,100 °C). For comparison, two other electrocatalysts (A-1000-1000 and NA-350-1000), either without low-temperature pre-carbonization or activated in the absence of $ZnCl_2$, were also prepared. Herein, all the prepared electrocatalysts were named as A/NA-T_1-T_2, where A, NA, T_1, and T_2 represent activation by $ZnCl_2$, activation without the addition of $ZnCl_2$, the pre-carbonization temperature, and the activation temperature, respectively.

As expected, all the prepared electrocatalysts exhibit amorphous graphitic structure as indicated by two characteristic peaks at 24° and 44° in X-ray diffraction patterns (Fig. S2 in the ESM) [28]. High-resolution transmission electron microscopy (TEM) studies, as exampled by the A-350-1000 electrocatalyst, also indicate the amorphous structure of the obtained catalysts (Fig. S3 in the ESM). Morphologically, all the derived catalysts have similar granular shape (Fig. S4 in the ESM), while their microporous structures are different (Figs. S5 and S6 in the

ESM). Specifically, the N_2 adsorption–desorption results (Figs. S5 and S6 in the ESM) show that the A-350-T_2 electrocatalysts have much larger Brunauer–Emmett–Teller (BET) surface areas and total pore volumes than the electrocatalysts prepared either without low-temperature pre-carbonization (A-1000-1000) or activated in the absence of $ZnCl_2$ (NA-350-1000). These results reveal the importance of each step in the two-step carbonization, where the low-temperature pre-carbonization can maintain the framework of carbon structure with slight shrinkage (Fig. S7 in the ESM), and the subsequent $ZnCl_2$ activation can efficiently enhance the porosity of the electrocatalysts.

3.2 Catalytic performances of carbon electrocatalysts

Next, we tested the electrocatalysts for CO_2RR by LSV in an aqueous solution of $KHCO_3$ (0.1 mol·L^{-1}). According to the linear sweep voltammetry studies (Fig. 1(b) and Fig. S8 in the ESM), all the obtained electrocatalysts possess the activity for CO_2RR in a certain potential range as indicated by the higher current in the CO_2 environment than that in the Ar environment. Particularly, the A-350-1000 and A-350-1100 electrocatalysts exhibit the most positive onset potential and relatively high reducing current (Fig. 1(b)), indicating better catalytic activities of the A-350-1000 and A-350-1100 electrocatalysts than those of other catalysts.

We then evaluated the catalytic performance of the obtained electrocatalysts for CO_2RR by analysing the electroreduction products under constant potentials (Figs. 1(c) and 1(d) and Fig. S9 in the ESM). Notably, no liquid product was observed, and therefore only gaseous products, including H_2 and CO, were considered. As indicated by the FE_{CO} (Fig. 1(c)) and CO partial current density (j_{CO}, Fig. 1(d)), the selectivity and activity of the electrocatalysts have potential dependence. At the potential of −1.09 V (indicated in Figs. 1(c) and 1(d) by dashed lines), the A-350-1000 and A-350-1100 electrocatalysts can give a FE_{CO} of ~ 89% and 87%, respectively, indicating high CO selectivity and suppression on H_2 evolution (Fig. 1(c) and Fig. S9 in the ESM). In addition, our control experiments confirm that the generation of CO is attributed to the CO_2 reduction catalyzed by the electrocatalysts (Fig. S10 in the ESM). Noteworthily, the NA-350-1000 and A-1000-1000 catalysts, used as control catalysts, have low activity and selectivity for CO_2RR, indicating the importance of both the low-temperature pre-carbonization and $ZnCl_2$ activation during the preparation of catalysts. Considering the high CO_2RR selectivity of A-350-1000 at −1.09 V and its relatively lower temperature required in preparation than that of A-350-1100, we thus regard the A-350-1000 as the best electrocatalyst for CO_2RR in this study.

In an attempt to study the stability of the electrocatalysts, we continuously performed the electroreduction of CO_2 by using the A-350-1000 electrocatalyst at the potential of −1.09 V for ~ 10 days (Fig. 1(e)). Inspiringly, the FE_{CO} maintained well at 86.9% ± 3.5% in 231 h, presenting a stable performance of the A-350-1000 electrocatalyst. Meanwhile, the H_2 Faradaic efficiency remained less than < 20% during the long term test. To the best of our knowledge, the stability of A-350-1000 can be viewed as excellent when compared with the reported carbon-based electrocatalysts in the literatures (Table S1 in the ESM).

3.3 Identifying active sites on carbon electrocatalysts for CO_2RR

In the following sets of experiments, we tried to identify the catalytically active sites which are responsible for the efficient and stable performance of the obtained A-350-1000 electrocatalyst. On a separate note, the adsorption of CO_2 on electrocatalysts can contribute to improving the performance of electrocatalysts for CO_2RR [32]. Considering the large surface areas and abundant micropores of the A-350-T_2 electrocatalysts, we measured the physisorbed CO_2 on the obtained electrocatalysts. As anticipated, the A-350-T_2 electrocatalysts can adsorb more CO_2 molecules than the two control catalysts (A-1000-1000 and NA-350-1000) (Figs. S11–S13 in the ESM). However, all the A-350-T_2 electrocatalysts have almost the same CO_2 adsorption capability, while they exhibit disparate catalytic properties for CO_2RR (Fig. 1(c) and 1(d) and Fig. S13 in the ESM). Consistently, the electrochemically active surface area (ECSA) of the electrocatalysts, an indicator for evaluating the reaction interface between the electrocatalyst and CO_2 molecules in the electrolyte, shows a similar trend (Figs. S14 and S15 in the ESM). These results imply that other than CO_2 adsorption, other crucial factors should contribute to the electroreduction of CO_2 when the A-350-T_2 electrocatalysts are applied.

Zn remaining in the A-350-T_2 electrocatalysts can be the possible active sites for CO_2RR due to the addition of $ZnCl_2$ for the high temperature activation [33–35]. Indeed, the quantitative analysis of Zn in the A-350-T_2 electrocatalysts by inductively coupled plasma mass spectrometry (ICP-MS) reveals the presence of Zn residues (Fig. 2(a)), and the amount of Zn

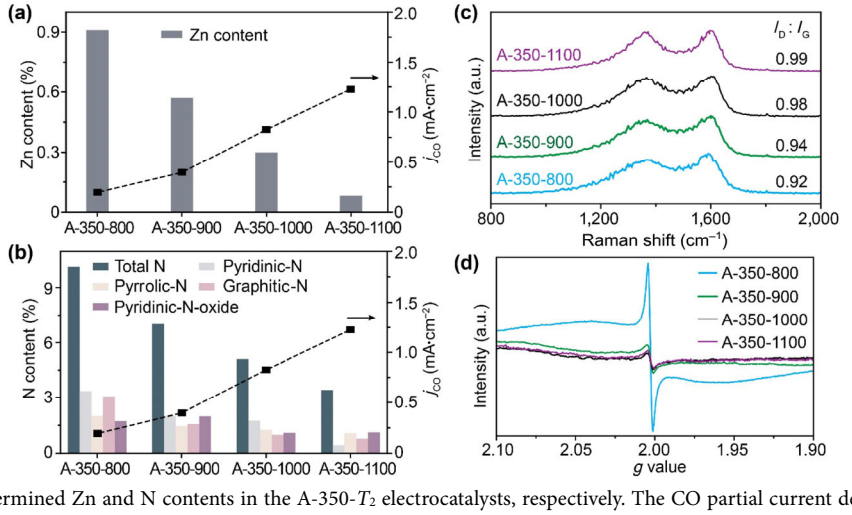

Figure 2 (a) and (b) Determined Zn and N contents in the A-350-T_2 electrocatalysts, respectively. The CO partial current densities (j_{CO}) at −1.09 V by using the A-350-T_2 electrocatalysts are also plotted as square dots in (a) and (b) for comparison, and the dashed lines are the guide for the eye. (c) and (d) Raman and room temperature electron paramagnetic resonance spectra of the A-350-T_2 electrocatalysts, respectively.

in the catalysts decreases with the increase of activation temperature. Despite the presence of Zn residues, the catalytic performance of the A-350-T_2 electrocatalysts increases with the decrease of Zn residues as indicated by the j_{CO} (Fig. 2(a)). In addition, using the A-350-1000 electrocatalyst as an example, we tried to remove Zn residues as many as possible by prolonging the acid washing time. The amount of Zn residues did decrease with the increase of washing time, while the catalytic performance of the electrocatalyst almost remained intact (Fig. S16 in the ESM). Taken together, these results indicate that Zn residues in the A-350-T_2 electrocatalysts play an almost negligible role during the electroreduction of CO_2. On a separate note, the biomass-derived carbon may contain other metal elements (e.g., Fe, Co, Ni and Cu) because of the natural precursor. Herein, we examined the metal contents by ICP-MS, and it was found that these metals are at negligible levels (Table S2 in the ESM). We therefore reason that metal elements should not be the dominant active sites.

We then checked the N contents in the A-350-T_2 electrocatalysts because the N doped in carbon-based catalysts can introduce active sites, either negatively-charged N atoms [32, 36, 37] or positively-charged C atoms [6, 38], for CO_2 adsorption and reduction. X-ray photoelectron spectroscopy (XPS) analyses of the N contents in the A-350-T_2 electrocatalysts show that the total amount of N element decreases with the increase of activation temperature (Fig. 2(b) and Figs. S17 and S18 in the ESM). Moreover, as revealed by the deconvolution of high-resolution XPS spectra for N 1s (Fig. 2(b) and Fig. S18 in the ESM), the pyridinic N and graphitic N, which are suggested to be active sites for CO_2RR [32], also become less when the activation temperature increases. By correlating the j_{CO} with the amount of N contents, we observed that the catalytic performance of A-350-T_2 electrocatalysts became better with the decrease of N contents (Fig. 2(b) and Fig. S19 in the ESM). Collectively, we believe that the N atoms in the A-350-T_2 electrocatalysts should not be the main active sites for CO_2RR.

Subsequently, inspired by the high activation temperature causing decrease of N contents in the A-350-T_2 electrocatalysts, we checked the intrinsic defects in the obtained electrocatalysts. It should be emphasized that intrinsic defects can be created in the carbon matrix by eliminating doped N atoms at high temperature [29]. As shown in Fig. 2(c), the A-350-T_2 electrocatalysts have two Raman bands, namely D (~ 1,360 cm^{-1}) and G (~ 1,600 cm^{-1}) bands, and the intensity ratio of D to G band (I_D/I_G) maintains at ~ 1 (Fig. 2(c)). Typically, the D band and G band can be correlated to the intrinsic defects in the carbon matrix and the graphitic structure of carbon materials, respectively. The I_D/I_G thus can indicate the abundance of intrinsic defects in carbon-based catalysts [28]. Taking previous studies into account [21], we believe that the A-350-T_2 electrocatalysts possess abundant intrinsic defects at a similar level.

Despite the similar abundance of intrinsic defects in the A-350-T_2 electrocatalysts, our electron paramagnetic resonance (EPR) studies suggest that the A-350-T_2 electrocatalysts activated at different temperatures have different types of defects in the carbon matrix (Fig. 2(d) and Fig. S20 in the ESM). According to the analysis of the EPR spectra, we can deduce that the A-350-800 and A-350-900 electrocatalysts with low catalytic activity have many defects that possess unpaired electrons, such as dangling bonds and single vacancies. Meanwhile, the A-350-1000 and A-350-1100 electrocatalysts with high catalytic activity are rich in the sp^2 ring defects in the carbon plane, such as Stone-Wales (5,775), octagonal (585), and pentagon defects. In addition, we tried to directly observe the defects by aberration-corrected TEM. Some clues of the sp^2 ring defects in the carbon plane of the A-350-1000 electrocatalyst could be deduced, while it was difficult to directly image these defects (Fig. S21 in the ESM). Taking all the aforementioned results together, we believe that the good catalytic performance of the prepared electrocatalysts should be mainly attributed to the abundant sp^2 ring defects in the carbon matrix.

3.4 Reaction pathways of CO_2RR on carbon electrocatalysts

To gain deeper insights, we then applied theoretical calculations to study the roles of sp^2 ring defects during the electroreduction of CO_2. Prior to the calculations, we employed electrochemical methods to identify the pathway of CO_2RR, particularly the rate-determining step, on the basis of previously proposed CO_2-to-CO mechanisms (Fig. 3 and computational details in the ESM) [39]. Briefly, using the A-350-1000 electrocatalyst as a representative, electrochemical impedance spectroscopy (EIS) shows that the charge transfer impendence, as indicated by the circle at the low frequency range, becomes lower when the applied potential decreases from −0.79 to −1.09 V (Fig. 3(a)). The lower charge transfer impedance corresponds well with better catalytic performance (Figs. 1(c) and 1(d)), indicating that a certain charge transfer step plays an important role in the catalysis of CO_2RR. Meanwhile, a Tafel slope of 111 mV·dec^{-1} was obtained (Fig. 3(b)), revealing that the rate-determining step is the initial single electron transfer to CO_2 [38, 40]. In addition, we found that the j_{CO} almost has no dependence on

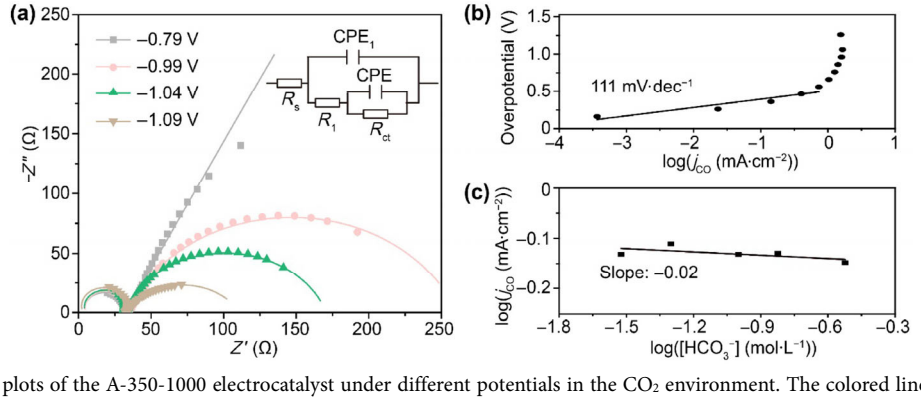

Figure 3 (a) Nyquist plots of the A-350-1000 electrocatalyst under different potentials in the CO_2 environment. The colored lines are simulated results according to the equivalent electrical circuit inserted in (a). In the equivalent electrical circuit, R_{ct} and CPE are related to the Faradaic charge-transfer process, R_1 and CPE_1 are related to the non-Faradaic CO_2 adsorption on the electrode, and R_s is the Ohmic resistance. (b) Tafel plot of the A-350-1000 electrocatalyst in the CO_2 environment. (c) log–log plot of the j_{CO} against the concentration of HCO_3^- ([HCO_3^-]) by using the A-350-1000 electrocatalyst at −1.09 V.

the concentration of HCO_3^- (Fig. 3(c)). Considering that the concentration of HCO_3^- can affect the local pH near the reaction interface [41], we here propose that the rate-determining step is the initial direct electron transfer step, forming the $CO_2^{\bullet-}$ intermediate, and the acceleration of reaction kinetics should be related to this step (see computational details in the ESM).

Based on the proposed pathway of CO_2RR, we simulated the rate-determining step, namely the formation of $*CO_2^-$ intermediate through an electron transfer, by the wave-function based computation (computational details in the ESM). Four fragment models with typically observed structures and sp^2 ring defects in carbon materials were constructed (Fig. 4(a)). Specifically, the four models with nine selected potential active sites can represent pristine graphene with zigzag and armchair edges, pentagon defect in plane, 5775 defect as well as 585 defect at the edge, respectively. The free energy changes of $*CO_2^-$ formation, ΔG_{ET}, were calculated by using a CO_2 electrode as the reference. As shown in Fig. 4(b), all the defective sites (sites 4–9 in Fig. 4(a)) exhibit negative values of free energy, indicating that CO_2 reduction can be significantly promoted by the topological defects in carbon matrix. These calculation results can correspond well with our experimental observations, suggesting that our two-step carbonization method can produce carbon-based electrocatalysts with intrinsic defects for efficient CO_2RR.

4 Conclusion

In summary, we have demonstrated a two-step carbonization approach for fabricating carbon-based defect-rich electrocatalysts with efficient and stable performance for CO_2 reduction. Importantly, our combined experimental and theoretical studies reveal that the intrinsic defects, together with the facilitated CO_2 adsorption and direct electron transfer pathway, mainly contribute to the good performance of the biomass derived electrocatalysts. Considering that the method can also convert other biomaterials such as egg white into electrocatalysts with similar performance (Figs. S22 and S23 in the ESM), we believe that our demonstration should pave the way for large-scale synthesis of carbon-based electrocatalysts from biomass in a low-cost way. We also envision that our findings shown here, combined with recent advances in reaction mechanisms of CO_2 reduction, can facilitate the practical applications of the CO_2 electroreduction.

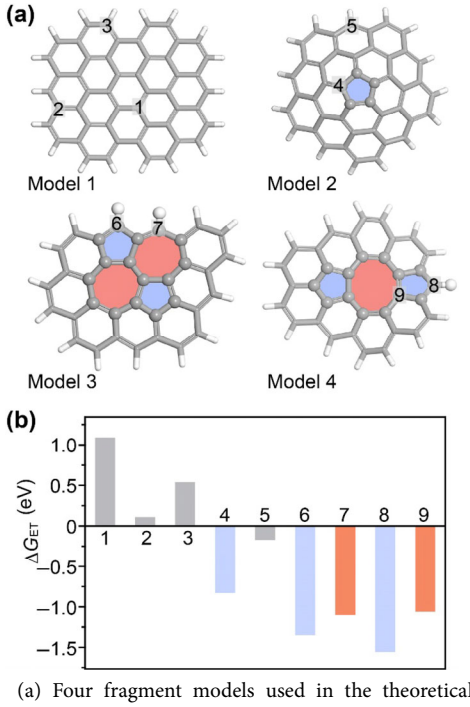

Figure 4 (a) Four fragment models used in the theoretical studies. Defective rings are highlighted in color. (b) Calculated free energy change of the $*CO_2^-$ formation (ΔG_{ET}) on representative sites as marked in (a).

Acknowledgements

The authors thank the National Key R&D Program of China (No. 2017YFA0207201), Six Talent Peaks Project in Jiangsu Province (No. JNHB-038), and Young Elite Scientists Sponsorship Program by CAST (No. 2017QNRC001) for financial support.

Electronic Supplementary Material: Supplementary material (including experimental details, calculation details and supplementary figures) is available in the online version of this article at https://doi.org/10.1007/s12274-020-2683-2

References

[1] Sun, T. T.; Xu, L. B.; Wang, D. S.; Li, Y. D. Metal organic frameworks derived single atom catalysts for electrocatalytic energy conversion. *Nano Res*. **2019**, *12*, 2067–2080.

[2] Song, R. B.; Zhu, W. L.; Fu, J. J.; Chen, Y.; Liu, L.; Zhang, J. R.; Lin, Y.; Zhu, J. J. Electrode materials engineering in electrocatalytic CO_2 reduction: Energy input and conversion efficiency. *Adv. Mater*., in press, DOI: 10.1002/adma.201903796.

[3] Wu, J. J.; Sharifi, T.; Gao, Y.; Zhang, T. Y.; Ajayan, P. M. Emerging carbon-based heterogeneous catalysts for electrochemical reduction of carbon dioxide into value-added chemicals. *Adv. Mater*. **2019**, *31*, 1804257.

[4] Zhu, D. D.; Liu, J. L.; Qiao, S. Z. Recent advances in inorganic heterogeneous electrocatalysts for reduction of carbon dioxide. *Adv. Mater*. **2016**, *28*, 3423–3452.

[5] Lin, R.; Ma, X. L.; Cheong, W. C.; Zhang, C.; Zhu, W.; Pei, J. J.; Zhang, K. Y.; Wang, B.; Liang, S. Y.; Liu, Y. X. et al. PdAg bimetallic electrocatalyst for highly selective reduction of CO_2 with low COOH* formation energy and facile CO desorption. *Nano Res*. **2019**, *12*, 2866–2871.

[6] Kumar, B.; Asadi, M.; Pisasale, D.; Sinha-Ray, S.; Rosen, B. A.; Haasch, R.; Abiade, J.; Yarin, A. L.; Salehi-Khojin, A. Renewable and metal-free carbon nanofibre catalysts for carbon dioxide reduction. *Nat. Commun*. **2013**, *4*, 2819.

[7] Liu, X.; Dai, L. M. Carbon-based metal-free catalysts. *Nat. Rev. Mater*. **2016**, *1*, 16064.

[8] Yan, X. C.; Jia, Y.; Yao, X. D. Defects on carbons for electrocatalytic oxygen reduction. *Chem. Soc. Rev*. **2018**, *47*, 7628–7658.

[9] Yan, X. C.; Jia, Y.; Odedairo, T.; Zhao, X. J.; Jin, Z.; Zhu, Z. H.; Yao, X. D. Activated carbon becomes active for oxygen reduction and hydrogen evolution reactions. *Chem. Commun*. **2016**, *52*, 8156–8159.

[10] Zhang, S.; Kang, P.; Ubnoske, S.; Brennaman, M. K.; Song, N.; House, R. L.; Glass, J. T.; Meyer, T. J. Polyethylenimine-enhanced electrocatalytic reduction of CO_2 to formate at nitrogen-doped carbon nanomaterials. *J. Am. Chem. Soc*. **2014**, *136*, 7845–7848.

[11] Wang, H. X.; Chen, Y. B.; Hou, X. L.; Ma, C. Y.; Tan, T. W. Nitrogen-doped graphenes as efficient electrocatalysts for the selective reduction of carbon dioxide to formate in aqueous solution. *Green Chem*. **2016**, *18*, 3250–3256.

[12] Kuang, M.; Guan, A. X.; Gu, Z. X.; Han, P.; Qian, L. P.; Zheng, G. F. Enhanced N-doping in mesoporous carbon for efficient electrocatalytic CO_2 conversion. *Nano Res*. **2019**, *12*, 2324–2329.

[13] Wu, J. J.; Ma, S. C.; Sun, J.; Gold, J. I.; Tiwary, C. S.; Kim, B.; Zhu, L. Y.; Chopra, N.; Odeh, I. N.; Vajtai, R. et al. A metal-free electrocatalyst for carbon dioxide reduction to multi-carbon hydrocarbons and oxygenates. *Nat. Commun*. **2016**, *7*, 13869.

[14] Cui, X. Q.; Pan, Z. Y.; Zhang, L. J.; Peng, H. S.; Zheng, G. F. Selective etching of nitrogen-doped carbon by steam for enhanced electrochemical CO_2 reduction. *Adv. Energy Mater*. **2017**, *7*, 1701456.

[15] Ghausi, M. A.; Xie, J. F.; Li, Q. H.; Wang, X. Y.; Yang, R.; Wu, M.; Wang, Y.; Dai, L. CO_2 overall splitting by a bifunctional metal-free electrocatalyst. *Angew. Chem., Int. Ed.* **2018**, *57*, 13135–13139.
[16] Chen, Z. P.; Mou, K. W.; Yao, S. Y.; Liu, L. C. Highly selective electrochemical reduction of CO_2 to formate on metal-free nitrogen-doped PC61BM. *J. Mater. Chem. A* **2018**, *6*, 11236–11243.
[17] Li, H. Q.; Xiao, N.; Hao, M. Y.; Song, X. D.; Wang, Y. W.; Ji, Y. Q.; Liu, C.; Li, C.; Guo, Z.; Zhang, F. et al. Efficient CO_2 electroreduction over pyridinic-N active sites highly exposed on wrinkled porous carbon nanosheets. *Chem. Eng. J.* **2018**, *351*, 613–621.
[18] Tuci, G.; Filippi, J.; Ba, H.; Rossin, A.; Luconi, L.; Pham-Huu, C.; Vizza, F.; Giambastiani, G. How to teach an old dog new (electrochemical) tricks: Aziridine-functionalized CNTs as efficient electrocatalysts for the selective CO_2 reduction to CO. *J. Mater. Chem. A* **2018**, *6*, 16382–16389.
[19] Hursán, D.; Samu, A. A.; Janovák, L.; Artyushkova, K.; Asset, T.; Atanassov, P.; Janáky, C. Morphological attributes govern carbon dioxide reduction on N-doped carbon electrodes. *Joule* **2019**, *3*, 1719–1733.
[20] Wang, W.; Shang, L.; Chang, G. J.; Yan, C. Y.; Shi, R.; Zhao, Y. X.; Waterhouse, G. I. N.; Yang, D. J.; Zhang, T. R. Intrinsic carbon-defect-driven electrocatalytic reduction of carbon dioxide. *Adv. Mater.* **2019**, *31*, 1808276.
[21] Jia, Y.; Zhang, L. Z.; Zhuang, L. Z.; Liu, H. L.; Yan, X. C.; Wang, X.; Liu, J. D.; Wang, J. C.; Zheng, Y. R.; Xiao, Z. H. et al. Identification of active sites for acidic oxygen reduction on carbon catalysts with and without nitrogen doping. *Nat. Catal.* **2019**, *2*, 688–695.
[22] Titirici, M. Defects win over pyridinic sites. *Nat. Catal.* **2019**, *2*, 642–643.
[23] Zhu, J. W.; Huang, Y. P.; Mei, W. C.; Zhao, C. Y.; Zhang, C. T.; Zhang, J.; Amiinu, I. S.; Mu, S. C. Effects of intrinsic pentagon defects on electrochemical reactivity of carbon nanomaterials. *Angew. Chem., Int. Ed.* **2019**, *58*, 3859–3864.
[24] Jiang, Y. F.; Yang, L. J.; Sun, T.; Zhao, J.; Lyu, Z. Y.; Zhuo, O.; Wang, X. Z.; Wu, Q.; Ma, J.; Hu, Z. Significant contribution of intrinsic carbon defects to oxygen reduction activity. *ACS Catal.* **2015**, *5*, 6707–6712.
[25] Daiyan, R.; Tan, X.; Chen, R.; Saputera, W. H.; Tahini, H. A.; Lovell, E.; Ng, Y. H.; Smith, S. C.; Dai, L. M.; Lu, X. Y. et al. Electroreduction of CO_2 to CO on a mesoporous carbon catalyst with progressively removed nitrogen moieties. *ACS Energy Lett.* **2018**, *3*, 2292–2298.
[26] Li, W. L.; Herkt, B.; Seredych, M.; Bandosz, T. J. Pyridinic-N groups and ultramicropore nanoreactors enhance CO_2 electrochemical reduction on porous carbon catalysts. *Appl. Catal. B: Environ.* **2017**, *207*, 195–206.
[27] Li, F. W.; Xue, M. Q.; Knowles, G. P.; Chen, L.; MacFarlane, D. R.; Zhang, J. Porous nitrogen-doped carbon derived from biomass for electrocatalytic reduction of CO_2 to CO. *Electrochim. Acta* **2017**, *245*, 561–568.
[28] Lu, M.; Qian, Y. J.; Yang, C. C.; Huang, X.; Li, H.; Xie, X. J.; Huang, L.; Huang, W. Nitrogen-enriched pseudographitic anode derived from silk cocoon with tunable flexibility for microbial fuel cells. *Nano Energy* **2017**, *32*, 382–388.
[29] Cho, S. Y.; Yun, Y. S.; Lee, S.; Jang, D.; Park, K. Y.; Kim, J. K.; Kim, B. H.; Kang, K.; Kaplan, D. L.; Jin, H. J. Carbonization of a stable β-sheet-rich silk protein into a pseudographitic pyroprotein. *Nat. Commun.* **2015**, *6*, 7145.
[30] Jones, F.; Tran, H.; Lindberg, D.; Zhao, L. M.; Hupa, M. Thermal stability of zinc compounds. *Energy Fuels* **2013**, *27*, 5663–5669.
[31] Caturla, F.; Molina-Sabio, M.; Rodríguez-Reinoso, F. Preparation of activated carbon by chemical activation with $ZnCl_2$. *Carbon* **1991**, *29*, 999–1007.
[32] Liu, S.; Yang, H. B.; Huang, X.; Liu, L. H.; Cai, W. Z.; Gao, J. J.; Li, X. N.; Zhang, T.; Huang, Y. Q.; Liu, B. Identifying active sites of nitrogen-doped carbon materials for the CO_2 reduction reaction. *Adv. Funct. Mater.* **2018**, *28*, 1800499.
[33] Won, D. H.; Shin, H.; Koh, J.; Chung, J.; Lee, H. S.; Kim, H.; Woo, S. I. Highly efficient, selective, and stable CO_2 electroreduction on a hexagonal Zn catalyst. *Angew. Chem., Int. Ed.* **2016**, *55*, 9297–9300.
[34] Yang, F.; Song, P.; Liu, X. Z.; Mei, B. B.; Xing, W.; Jiang, Z.; Gu, L.; Xu, W. L. Highly efficient CO_2 electroreduction on ZnN_4-based single-atom catalyst. *Angew. Chem., Int. Ed.* **2018**, *57*, 12303–12307.
[35] Wu, Y. S.; Jiang, J. B.; Weng, Z.; Wang, M. Y.; Broere, D. L. J.; Zhong, Y. R.; Brudvig, G. W.; Feng, Z. X.; Wang, H. L. Electroreduction of CO_2 catalyzed by a heterogenized Zn-porphyrin complex with a redox-innocent metal center. *ACS Cent. Sci.* **2017**, *3*, 847–852.
[36] Song, Y. F.; Chen, W.; Zhao, C. C.; Li, S. G.; Wei, W.; Sun, Y. H. Metal-free nitrogen-doped mesoporous carbon for electroreduction of CO_2 to ethanol. *Angew. Chem., Int. Ed.* **2017**, *56*, 10840–10844.
[37] Wang, R. M.; Sun, X. H.; Ould-Chikh, S.; Osadchii, D.; Bai, F.; Kapteijn, F.; Gascon, J. Metal-organic-framework-mediated nitrogen-doped carbon for CO_2 electrochemical reduction. *ACS Appl. Mater. Interfaces* **2018**, *10*, 14751–14758.
[38] Wang, H.; Jia, J.; Song, P. F.; Wang, Q.; Li, D. B.; Min, S. X.; Qian, C. X.; Wang, L.; Li, Y. F.; Ma, C. et al. Efficient electrocatalytic reduction of CO_2 by nitrogen-doped nanoporous carbon/carbon nanotube membranes: A step towards the electrochemical CO_2 refinery. *Angew. Chem., Int. Ed.* **2017**, *56*, 7847–7852.
[39] Lee, C. W.; Cho, N. H.; Im, S. W.; Jee, M. S.; Hwang, Y. J.; Min, B. K.; Nam, K. T. New challenges of electrokinetic studies in investigating the reaction mechanism of electrochemical CO_2 reduction. *J. Mater. Chem. A* **2018**, *6*, 14043–14057.
[40] Medina-Ramos, J.; DiMeglio, J. L.; Rosenthal, J. Efficient reduction of CO_2 to CO with high current density using *in situ* or *ex situ* prepared bi-based materials. *J. Am. Chem. Soc.* **2014**, *136*, 8361–8367.
[41] Wuttig, A.; Yoon, Y.; Ryu, J.; Surendranath, Y. Bicarbonate is not a general acid in Au-catalyzed CO_2 electroreduction. *J. Am. Chem. Soc.* **2017**, *139*, 17109–17113.